



International Journal of Nanotechnology

ISSN online: 1741-8151 - ISSN print: 1475-7435

<https://www.inderscience.com/ijnt>

Small cell lung tumour differentiation using F-18 (Fluorine-18) PET and smoothing using Gaussian 3D convolution operator

J. Vijayaraj, D. Loganathan, T.P. Latchoumi, M. Venkata Pavan, P. Jhansi Lakshmi

DOI: [10.1504/IJNT.2023.10056471](https://doi.org/10.1504/IJNT.2023.10056471)

Article History:

Received: 14 April 2021

Last revised: 08 June 2021

Accepted: 09 June 2021

Published online: 31 May 2023

Small cell lung tumour differentiation using F-18 (Fluorine-18) PET and smoothing using Gaussian 3D convolution operator

J. Vijayaraj and D. Loganathan

Department of Computer Science and Engineering,
Pondicherry Engineering College,
Puducherry, 605014, India
Email: vijayaraj.j@eec.srmrmp.edu.in
Email: drloganathan@pec.edu

T.P. Latchoumi*

Department of Computer Science and Engineering,
SRM Institute of Science and Technology,
Ramapuram, Chennai, 600089, India
Email: latchout@srmist.edu.in
*Corresponding author

M. Venkata Pavan

Department of Mechanical Engineering,
VFSTR (Deemed to be University),
Andhra Pradesh, 522213, India
Email: mvpavan27@gmail.com

P. Jhansi Lakshmi

Department of Computer Science and Engineering,
VFSTR (Deemed to be University),
Andhra Pradesh, 522213, India
Email: laxmi.jhansi@gmail.com

Abstract: The most common disease for smokers is lung cancer. The deadly type of lung cancer is Small Cell Lung Cancer (SCLC). Tumour identification becomes complicated these days. It is only in the final stage that this form of lung cancer can be detected. When the patient has some of the earlier symptoms of SCLC, they can be subjected to preliminary tests of cancer. So this paper presents the part of the identification of lung cancer by differentiating identified tumour cells using Fluorine-18 positron emission tomography (F-18 PET) and that can be smoothed using Gaussian 3D convolution operator. The performance analysis shows the lung image dataset showing differentiation of tumour cells by applying F-18 PET, smoothed image using Gaussian 3D convolution operator and simulation graphs for accuracy, sensitivity, precision which shows the improved accuracy and specificity using Gaussian 3D convolution operator.

Keywords: small cell lung cancer; tumour cell; Fluorine-18 positron emission tomography; Gaussian 3D convolution operator; simulation; performance analysis.

Reference to this paper should be made as follows: Vijayaraj, J., Loganathan, D., Latchoumi, T.P., Pavan, M.V. and Lakshmi, P.J. (2023) 'Small cell lung tumour differentiation using F-18 (Fluorine-18) PET and smoothing using Gaussian 3D convolution operator', *Int. J. Nanotechnol.*, Vol. 20, Nos. 1/2/3/4, pp.98–115.

Biographical notes: J. Vijayaraj pursuing his PhD in the Department of Computer Science and Engineering from Pondicherry Engineering College. His domain of research in image processing and medical imaging. He has published work in four international journals and two conferences. His other areas of specialisations are Big data, AI and WSN. He is a certified Microsoft Certified Professional (MCP) From Microsoft Corporation.

D. Loganathan is a Professor in the Department of Computer Science and Engineering in Pondicherry Engineering College. His area of specialisation is image processing and Information security.

T.P. Latchoumi received her PhD in Computer Science and Engineering from Sathyabama Institute of Science and Technology in 2019. She used to work at Christ College of Engineering and Technology (2010–2015). She worked at VFSTR (Deemed to be University) in Andhra Pradesh (2016–2021). Currently, she is working in SRMIST, Chennai. Her research interests include artificial intelligence, machine learning and sensor networks.

M. Venkata Pavan is a research scholar at the Department of Mechanical Engineering, Vignan's Foundation for Science, Technology and Research-Guntur, AP, India, since February 2018. He completed MTech program in machine design at JNTUH, Hyderabad, India (2014–2016) and completed his BTech graduation in aeronautical engineering at JNTU Kakinada.

P. Jhansi Lakshmi received her MTech in Computer Science and Engineering from Acharya Nagarjuna University, Guntur. She is pursuing a PhD at Vignan's Foundation for Science, Technology, and Research, Guntur. She is currently working as an Assistant Professor in the Department of Computer Science and Engineering at VFSTR Deemed to be University, India. She has published research papers at national and international conference proceedings and journals. Her research interests include data mining, data warehousing, and machine learning.

1 Introduction

Cancer can be described as uncontrolled cell growth that can spread throughout the body. There are red blood cells (RBCs) in our bodies. The main role is to provide all areas of the body with fresh O₂ with aid of blood flow, which makes blood look red. Tissue receives O₂ in the lungs only because of RBCs. The genetic material of erythrocytes is extremely haemoglobin concentrated. Cell membrane, which is the foundation of

psychological cell activity, consists of proteins and lipids. They may not contain any large part of the cell that contains haemoglobin [1].

About 20 lakhs per second of new RBCs are made. Cells are formed in bone marrow as well as rotate in arteries and veins across the body for approximately four months to and fro. It takes approximately 20 seconds for each rotation. Red blood cells are about 75% of cells and much of the blood concentration in the human body. In 1658, with an early microscope, young Dutch biologist Jan Swammerdam perfectly-identified it. Malignant lung tumour characterised by uncontrolled cell growth in lung tissues is lung cancer, also referred to as carcinoma.

Some cancers that are also referred to as primary lung cancers are carcinomas that originate in the lungs. (1) small-cell lung cancer, (2) non-small-cell lung cancer are two major forms of carcinoma. Coughing, weight loss, shortness of breath, and minute and extreme chest pains are the most common symptoms. The cycle of red blood cells (RBC) formation and degradation disturbs these cancer cells. Both the arrangement and the composition of the plasma membrane, i.e., the outer arrangement of the cell, are altered internally so that these RBCs do not die in compliance with the associated lifetime. As a consequence, RBC count begins to rise and more and more cell numbness accumulates, resulting in vein and artery shortening as well as eventual bursting. Via cough, etc., these results in blood [2].

Early detection of lung cancer is of paramount importance if high mortality rates are to deteriorate. To increase the early detection rate, the global lung screening programme aims to PET and computed tomography (CT) exams for most elderly groups at risk. While the use of invasive procedures makes it difficult for radiologists to detect lesions, signs hardly occur until the disease is advanced. Unfortunately, with a 5-year survival rate of 17.8% and for distant tumours, most lung cancer patients suffering at advanced stages end in dismal, just 4%. Genuine and reliable knowledge is the cornerstone of efforts to manage diseases.

Ingestion of cigarettes accounts for more than 85% of the epidemic. In reality, genetic conditions, exposure to environmental contaminants, second-hand smoke quickly inflate illness. The survival rate, as well as the quality of life, are escalated through remedies like chemotherapy, radiotherapy, surgery, epidermal receptive medicines. This approach is all about early and critical diagnostics with intelligent computational methods with many distortion removals by segmentation methods as well as algorithms, which are the root definition of image processing [3].

Because of the structure of cancer cells, where most cells converge, lung cancer prediction is the most difficult challenge. Methods of image analysis are also used for lung cancer estimation and early identification and treatment of lung cancer. As a result, numerous lung cancer characteristics are obtained from photos, approaches based on pattern recognition help predict lung cancer. Unchecked development of irregular cells in lung cancer begins in one or both lungs, usually in air passages. Abnormal cells do not expand into healthy lung tissue; they produce and shape tumours easily. Lung cancer cases are rising very quickly, according to the American Cancer Society, and approximately 14% of newly diagnosed cancers are lung cancer and are the world's leading cause of cancer death. Previous diagnosis reports showed that the majority of lung cancer patients are over 60 years of age [4].

The tumour can be benign or malignant. A tumour that can be removed and can be prevented from spreading in other parts of the body is a form of benign tumour. A tumour

that develops aggressively and spreads to other parts of the body is known as malignant. Although an invasive technique such as biopsy is used, medical imaging is chosen to see into the body because it is safe for the patient as well as comfortable. For diagnosis of nodules as well as treatment of lung cancer, Medical Imaging plays a very significant role. This is a more effective as well as efficient diagnostic process.

Various types of images are used in medical imaging, but due to better clarity, lower noise, and less blur, CT images are selected for the identification of lung pathology. A key characteristic of CT scan images is that the mean and variance of CT scan images can be determined very quickly. The method of identification is mainly divided into four parts: image enhancement, lung segmentation, extraction of features, and classification. As it needs many pre-processing steps, Lung Segmentation is known to be the most difficult part [5].

Differentiating the affected portion of cancer in the lungs and having the best solution to the problem are the most challenging tasks in the medical field. Doctors have several issues with accurately spotting cancer-affected areas in the lungs. Image processing can be a solution for this form of problem, in particular for the identification of areas affected by cancer in the lungs. Historical records on various types of lung cancer imaging are collected and MRI techniques are used by doctors and clinicians to classify cancer-affected regions in the lungs.

The human visual system conducts specific tasks to distinguish the colour difference between the affected region of cancer and the non-affected region of lung image. Very smart programming and a lot of computing power are required to detect the colour difference. Interpretation of data in form of an image by a variety of potential techniques is important for the detection of colour through techniques of image segmentation. Usually, an image is viewed as a two-dimensional series of brightness values, and shapes such as that of a photographic print, a slide, a TV screen, or a video frame are most generally represented. Image can be viewed optically or digitally using a computer. Image analysis involves a mixture of different fields of AI, such as fuzzy logic, pattern recognition, and machine learning. The basic technique (image processing) is used for the segmentation of images and further processing. Image segmentation layers may be distinguished as image comprehension, image classification, and image processing. Various techniques are used to remove cancer or infected portion of the lung [6].

2 Literature survey

Possibility for the fractal study of time interval contrast-enhanced computed tomography (CECT) images to discern between aggressive as well as non-aggressive malignant lung tumours (i.e., high and low metabolic tumours). The goal is to increase the accuracy of CT tumour diagnosis by recognising the malignant aggressiveness of lung tumours. As branching of blood vessels can be called a fractal operation, the study explores vascularised tumour regions with strong fractal characteristics. The study is conducted after injection of 15 patients with a contrast agent as well as the transformation of at least 11-time series CE CT photographs from each patient to fractal level and estimation of resulting lacunarity. Fractal texture characteristics were distributed over tumour area and quantitative classification demonstrated up to 83.3% precision in the distinction between advanced (aggressive) as well as early (nonaggressive) malignant tumours [7].

Increase accuracy of intraoperative ultra-sound (US) photographs of a deflated lung undergoing a minimally invasive ablative tumour procedure has been suggested. Since US images are very sensitive to residual air lingering in deflated lungs, US lung images are of very low quality and are thus not suited to image-guided procedures. Accurate as well as a high-quality intraoperative image of the lung is, therefore, a prime requirement for tumour localisation as well as fusion during such procedures with real-time navigation data. The suggested method utilises data from a preoperatively developed CT image of a deflated lung to improve that of US intraoperative images. Upgrading is carried out by two parallel registration schemes. Output is an improved US representation of deflated lung that is placed as well as situated correctly within its preoperative CT equivalent [8].

By making good use of superior contrast of PET images as well as the superior spatial resolution of CT images, they successfully combine two modalities. To solve the segmentation issue, random walk and graph cut method are combined, in which random walk is used as an initialisation tool to provide object seeds on PET as well as CT images for graph cut segmentation. The complexity of co-segmentation is conceived as an energy minimisation problem that is resolved by the max-flow/min-cut process. A graph is constructed comprising two sub-graphs and a special relationship in which one sub-graph is for PET and the other is for CT, and a particular relation is represented by a contextual word that penalises the difference between two forms of tumour segmentation. A novel energy representation is planned to completely leverage features of PET and CT images. Downhill expenses, as well as 3D derivative expenses, are suggested for PET. A shape penalty expense is inserted into the energy feature for CT, which during segmentation helps to reduce tumour area [9].

A tumour-customised downhill (TCD) technique is suggested to accomplish these aims. The solution includes: (1) automated specification of tumour-customised criteria to enhance the description of tumour borders, (2) monotonic property of uniform tumour uptake value (SUV) to distinguish tumour from neighbouring higher metabolism regions ('hot spot'), and 3) heterogeneity of the tumour. Method formulates the issue of segmentation of minimisation of a random field type of Markov, which encodes data from both modalities. Using a graph-cut based approach, optimisation is solved. For assessment, three simulated lesions and 30 PET-CT experiments were used, classified into 'simple' and 'complex' groups. Compared to a threshold based on 40% and 50% maximal SUV, adaptive threshold, fuzzy c-means, and watershed strategies (0.73) and 'complex' group (0.71); lowest volumetric error in 'simple' (1.76 mL) and 'complex' group (14.59 mL); highest average Dice similarity coefficient for simulation results data [10].

Propose a novel tumour co-segmentation approach in both PET as well as CT images that take advantage of the benefits of each modality: PET functionality data and CT anatomical structure information. Method formulates the issue of segmentation of minimisation of a random field type of Markov, which encodes data from both modalities. Using a graph-cut-based approach, optimisation is solved. For segmentation of PET and CT images respectively, two sub-graphs are constructed. To obtain reliable outcomes in two modalities, by adding context arcs between 2 sub-graphs, an adaptive context cost is applied. By solving a single maximal flow issue, which leads to simultaneous segmentation of tumour volumes in both modalities; an optimal solution can be obtained [11].

In positron emission tomography (PET) photos, we suggest a novel approach for single-channel blind separation of non-overlapping sources as well as to the best of our

understanding, extend it for the first time to automated segmentation of lung tumours. First of all, our approach transforms a 3D PET image into a pseudo multichannel view. Subsequently, to distinguish tumours from other tissues, regularisation-free sparseness controlled nonnegative matrix factorisation is used. We pick the tumour variable as one with minimum difficulty by using difficulty-based parameters. We contrasted the proposed method with criteria focused on 40% and 50% SUV, GC, RW, and AP algorithms on 18 non-small cell lung cancer datasets concerning ground reality provided by two radiologists [12].

Overview of lung cancer diagnosis, one of oncology's most important, interesting, overwhelming challenges. It is of significant scientific significance to establish a powerful CAD method for lung cancer that will improve the probability of survival for the patient. In a vast number of clinical trials, CAD schemes for lung cancer have been studied for this cause. Four major processing steps are composed of a standard CAD method for diagnosis of lung cancer: segmentation of lung fields, identification of nodules inside lung fields, segmentation of nodules found as well as diagnosis of nodules as benign or malignant. The latest state-of-art strategies developed to incorporate each of these CAD processing steps are overviewed in this paper. Various aspects of technical problems, methodologies adopted, records of preparation and testing, and methods of evaluation, as well as success achieved, are listed for each technique [13].

To address these concerns, it presents the use of neighbourhood as well as connectivity properties of CT image pixels. In this function, multiple morphological processing is used to eliminate lung CT image history, noises and airways then k-means clustering segmentation-based algorithms used for identification of lung tumours. Volumetric analysis of lung nodules according to the concept of TNM by WHO for tumour amounts measurement. TNM for lung cancer uses dimension, spread, and metastasis properties of tumours [14].

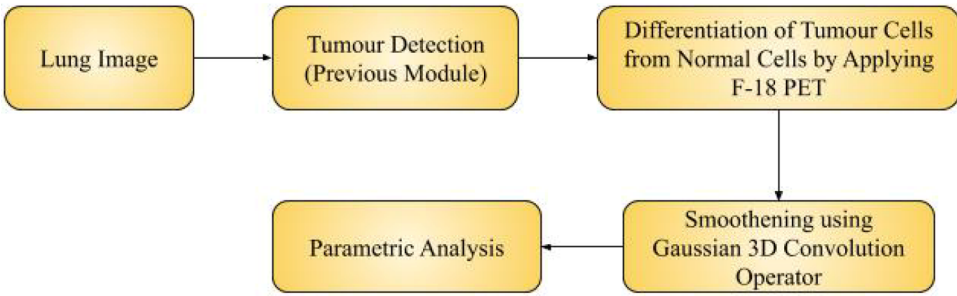
To enhance the precision of Fluorine-18 fluorodeoxyglucose (FDG-PET) in the diagnosis of lung malignancy, a procedure for developing an ideal dual time point 18F-FDG PET imaging protocol was suggested. Nonetheless, separate sampling timetables have been used, which makes clear comparisons with their studies challenging. It is unclear if these timetables have the same scope for diagnosis of lung malignancy, restricting further growth as well as application of these techniques. While malignant and benign lesions ideally display a differential in FDG uptake with longer periods of uptake, increasing noise due to decay will offset this profit as well as increase heterogeneity. The goal is to transfer the edge-preserving area noise smoothing paradigm to the methodology of texture-preserving LdCT image restoration while retaining the advantage of the MRF neighbourhood framework for edge preservation. In particular, the MRF model has been modified from previous FdCT scans to integrate image textures of skin, fat, bone, lung, etc. as a priori information for texture-preserving Bayesian reconstruction of existing LdCT images. Experiments using clinical patient scans were performed to demonstrate the viability of the current restoration system. In this function, multiple morphological processing is used to eliminate lung CT image history, noises and airways then k-means clustering segmentation-based algorithms used for identification of lung tumours. Experimental results revealed a drastic benefit from using widely used Haralick texture measurements in prior information for LdCT image reconstruction.

3 Research methodology

Previous lung cancer work has been carried out for the detection of tumour cells in the lung. And next module of this work has to be done for differentiation of tumour cells from normal cells by applying F-18 PET and can be smoothed using Gaussian 3D convolution operator which shows the differentiation of tumour cells.

As the tumour has been identified in the lungs, it needs to be differentiated from normal cells. So in this proposed method F18-PET is applied to differentiate the tumour cells. Then Gaussian 3D convolution operator has been used for the smoothing and can be viewed clearly. These steps are carried out at the earlier stages of SCLC as shown in Figure 1.

Figure 1 Proposed architecture (see online version for colours)



Parameter calculation/description:

PPV (positive predictive value)/ NP (negative predictive value) calculation:

$$\text{Positive}(TP)(FP) - TP + FP \text{ (Total number of subjects with a positive test)}$$

$$\text{Negative}(FN)(TN) - (FN) + (TN) \text{ (Total number of subjects with negative test)}$$

$$TP + FN \text{ (Total number of subjects with the given condition)}$$

$$FP + TN \text{ (Total number of subjects without given condition)}$$

$$N = TP + TN + FP + FN \text{ (Total number of subjects in study)}$$

$$\text{Specificity} = \frac{TN}{(TN + FP)} = \frac{\text{(Number of true negative assessment)}}{\text{(Number of all negative assessment)}}$$

$$\text{Accuracy} = \frac{TN + TP}{TN + TP + FN + FP} = \frac{\text{Number of correct assessments}}{\text{number of all assessment}}$$

Quantum noise: Amount of noise included in the image obtained from radiography images

Contrast detail analysis (CDA): it examines the physical parameters of the image such as the pixel size of the image. The quality of the image is estimated using CDA which is

considered an effective tool for processing. This provides quantitative evaluation between low contrast and small pixel measurement for medical images. CDA originated from the theory of signal detection and relies on low-contrast detail detection ability related to signal-to-noise ratio. The main concept behind this is noises from different sources affect the simulation performance of the image. Through which imaging system able to visualise small objects detection ability.

Gaussian 3D convolution operator:

$$G(x, y, z) = \frac{1}{2\pi\sigma^2} e^{-\frac{x^2+y^2+z^2}{2\sigma^2}} \tag{1}$$

Gaussian smoothing is performed with the 3D distribution of convolution through the 'point-spread function in $x, y,$ and x coordinate in Equation 1. Usually, PET images are in the form of discrete pixels which need to be approximated with Gaussian function. Based on theory Gaussian distribution is non-zero throughout the point which requires infinite convolution of the large kernel. However, in practice, it is zero after standard deviation and means, here the kernel needs to be truncated. An appropriate integer-valued convolution kernel with Gaussian is σ of 1.0. Here, it is not necessary to select values from mask values for Gaussian. The values can be chosen at the middle of the masked pixel, but due to non-linear pixel variance, these values are not reliable. It needs to be an integer of a pixel in Gaussian with increments of 0.001. But the image pixels are not an integer this can be rescaled into an array with a value of 1. In PET analysis final mask value is obtained as 273 for almost all selected sample images.

Figures 2–7 presented steps adopted in PET images for the proposed Gaussian 3D convolution operator.

Figure 2 Smoothed image 1 (see online version for colours)

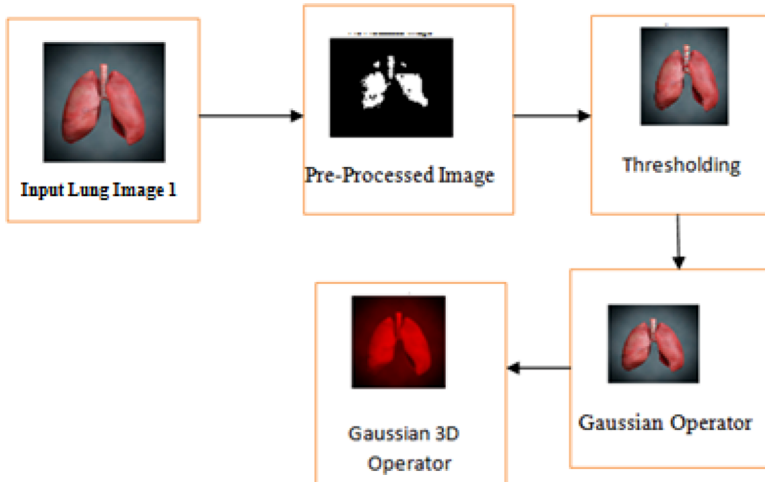


Figure 3 Smoothed image 2 (see online version for colours)

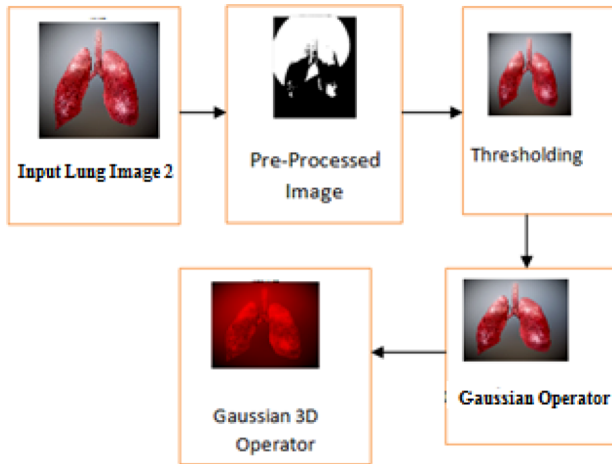


Figure 4 Smoothed image 3 (see online version for colours)

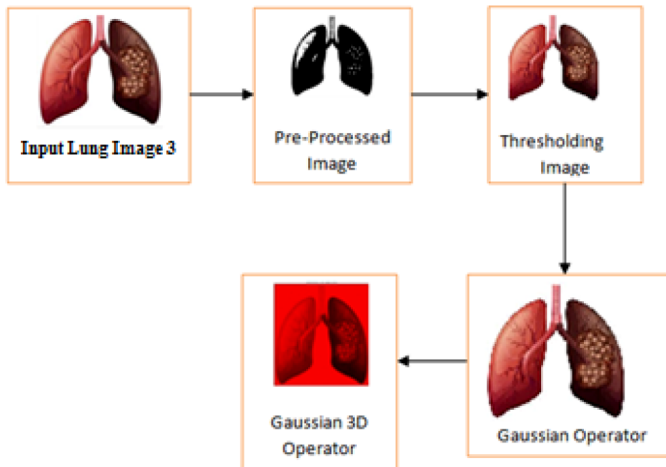


Figure 5 Smoothed image 4 (see online version for colours)

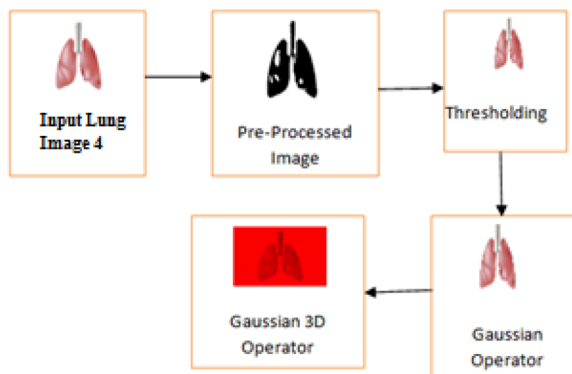


Figure 6 Smoothed image 5 (see online version for colours)

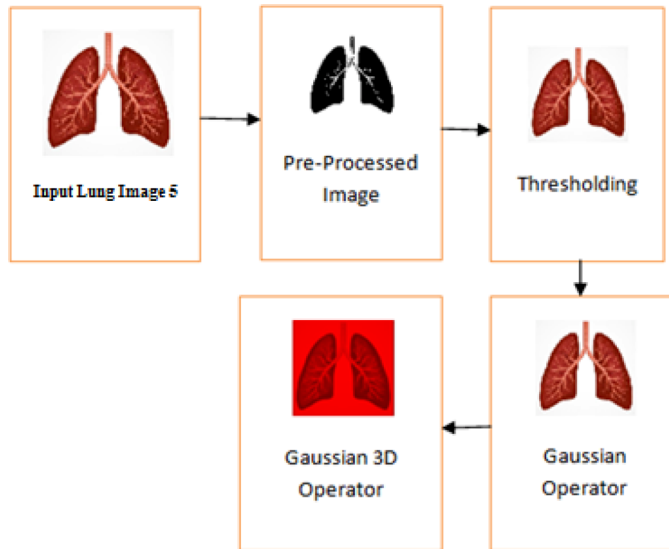
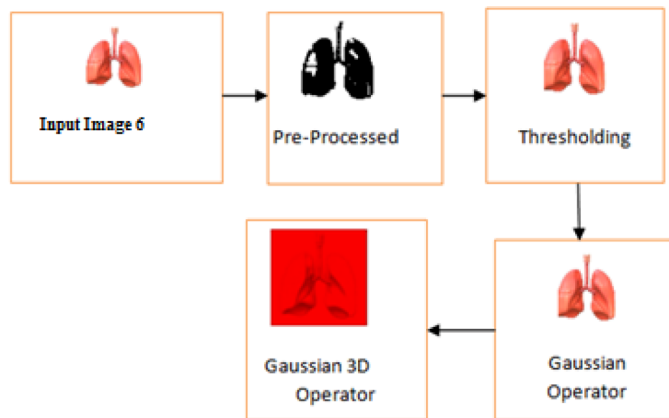


Figure 7 Smoothed image 6 (see online version for colours)



4 Performance analysis

Table 1 presents the performance of existing and proposed models for various parameters with image 1 whose pixel count is 256×256 .

Figure 8 shows a comparison of accuracy, specificity, sensitivity, precision, MSE, PSNR, PPV, NPV, quantum noise, and CDA for existing and proposed methods. *X* and *Y*-axes represent the parameters used and values obtained respectively. Red, blue, green yellow, pink, and orange colour indicate median filter, classifier, GSS filter, Kaun filter, 2D Euclidian operator, 3D convolution operator.

Table 1 Comparative performance analysis for image 1

Parameters used	Median filter	Classifier	Gaussian scale-space (GSS) filter	Kaun filter	Existing 2D Euclidean operator	3D convolution operator
Pixel count	256*256	256*256	256*256	256*256	256*256	256*256
Space	55.6	55.6	55.6	55.6	55.6	55.6
Accuracy	91.2	93.6	88	87	90.6	99.6
Specificity	89	87.5	86	83.4	79.4	98
Sensitivity	78.6	92.6	80.5	76.3	91.6	99.3
Precision	78	81.3	93.5	84.2	84.6	96
MSE	42.6	51.2	36.4	48.4	40.7	34.8
PSNR	47.5	62.5	48.6	38.6	44.2	30.7
PPV	88	76.5	82.6	76.2	88	96
NPV	67.8	77.2	83.5	74.6	80.6	87
Quantum noise	56.2	63.5	49.8	69.2	72.6	78
Contrast detail analysis	78.2	66.9	80.6	74.5	69.5	85

Figure 8 Comparison for image 1 with existing and proposed methods (see online version for colours)

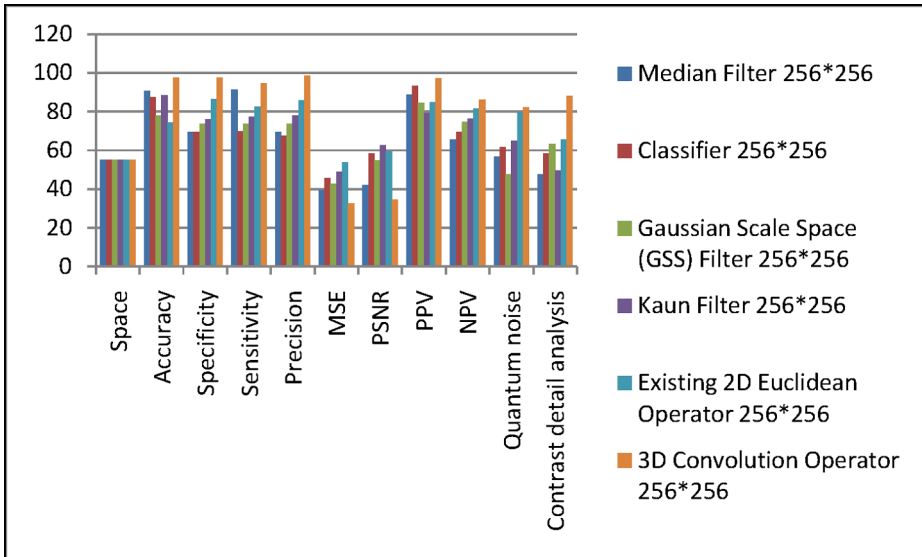


Table 2 presents the performance of existing and proposed models for various parameters with image 1 whose pixel count is 256×256 .

Table 2 Comparative performance analysis for image 2

<i>Parameters used</i>	<i>Median filter</i>	<i>Classifier</i>	<i>Gaussian scale-space (GSS) filter</i>	<i>Kaun filter</i>	<i>Existing 2D Euclidean operator</i>	<i>3D convolution operator</i>
Pixel count	256*256	256*256	256*256	256*256	256*256	256*256
Space	51.8	51.8	51.8	51.8	51.8	51.8
Accuracy	93.2	96.5	78.5	67	84.2	98.5
Specificity	78.6	81	92.6	86.2	87.5	97.3
Sensitivity	91.2	93.6	88.6	84.2	86.4	98
Precision	81	86.4	82.4	89.5	83.4	99
MSE	49.5	52.4	50.7	48.7	49.5	32.7
PSNR	36.7	45.7	40.7	57.2	38.6	30.7
PPV	88.7	78.6	62.8	57.4	63.5	99
NPV	67.5	73.6	81.6	79.6	80.6	86
Quantum noise	66.8	72.6	63.8	56.9	54.7	76
Contrast detail analysis	78.5	68.6	57.4	66.9	78.4	82

Figure 9 shows a comparison of accuracy, specificity, sensitivity, precision, MSE, PSNR, PPV, NPV, quantum noise, and CDA for existing and proposed methods. *X* and *Y*-axis represent the parameters used and values obtained respectively. Red, blue, green yellow, pink, and orange colour indicate median filter, classifier, GSS filter, Kaun filter, 2D Euclidean operator, 3D convolution operator.

Figure 9 Comparison for image 2 with existing and proposed methods (see online version for colours)

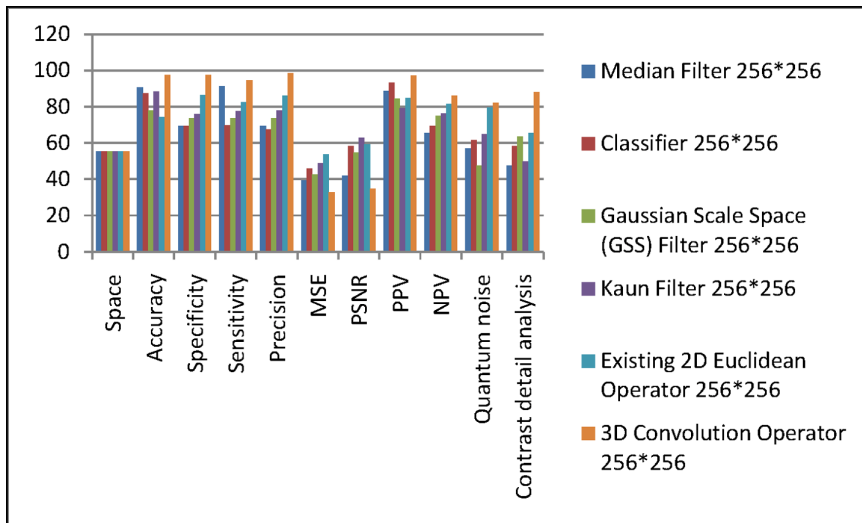


Table 3 presents the performance of existing and proposed models for various parameters with image 3 whose pixel count is 256×256 .

Table 3 Comparative performance analysis for image 3

Parameters used	Median filter	Classifier	Gaussian scale-space (GSS) filter	Kaun filter	Existing 2D Euclidean operator	3D convolution operator
Pixel count	256*256	256*256	256*256	256*256	256*256	256*256
Space	54	54	54	54	54	54
Accuracy	88.6	78.5	68.4	71.6	84.7	99.7
Specificity	84.2	86.3	91.3	81.4	79.5	99.4
Sensitivity	77.5	79.4	82.3	84.5	80.6	98
Precision	79	83.5	85.6	92.3	95.7	98
MSE	45.8	54.8	52.8	47.9	52.9	36.8
PSNR	44.9	49.7	52.9	63.7	58.6	36.8
PPV	88	74.6	72.9	86.3	76	98
NPV	77.6	79.4	58.6	62.7	68.4	81
Quantum noise	67.4	72.4	67.8	47.6	57.6	73
Contrast detail analysis	66.8	73.4	82.4	81.2	73.6	86

Figure 10 shows a comparison of accuracy, specificity, sensitivity, precision, MSE, PSNR, PPV, NPV, quantum noise, and CDA for existing and proposed methods. X and Y-axes represent the parameters used and values obtained respectively. Red, blue, green yellow, pink, and orange colour indicate median filter, classifier, GSS filter, Kaun filter, 2D Euclidean operator, 3D convolution operator. Table 4 presents the performance of existing and proposed models for various parameters with image 4 whose pixel count is 256×256 .

Figure 10 Comparison for image 3 with existing and proposed methods (see online version for colours)

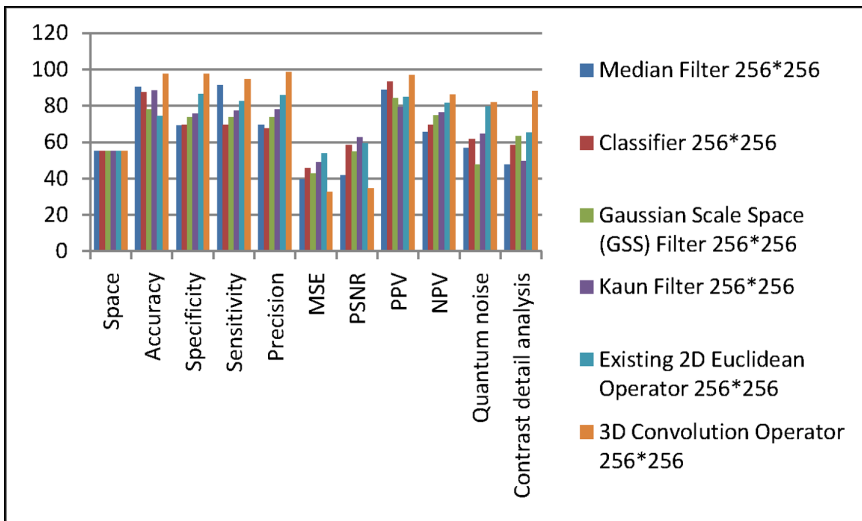


Table 4 Comparative performance analysis for image 4

<i>Parameters used</i>	<i>Median filter</i>	<i>Classifier</i>	<i>Gaussian scale-space (GSS) filter</i>	<i>Kaun filter</i>	<i>Existing 2D Euclidean operator</i>	<i>3D convolution operator</i>
Pixel count	256*256	256*256	256*256	256*256	256*256	256*256
Space	54	54	54	54	54	54
Accuracy	88.6	78.5	68.4	71.6	84.7	99.7
Specificity	84.2	86.3	91.3	81.4	79.5	99.4
Sensitivity	77.5	79.4	82.3	84.5	80.6	98
Precision	79	83.5	85.6	92.3	95.7	98
MSE	45.8	54.8	52.8	47.9	52.9	36.8
PSNR	44.9	49.7	52.9	63.7	58.6	36.8
PPV	88	74.6	72.9	86.3	76	98
NPV	77.6	79.4	58.6	62.7	68.4	81
Quantum noise	67.4	72.4	67.8	47.6	57.6	73
Contrast detail analysis	66.8	73.4	82.4	81.2	73.6	86

Figure 11 shows a comparison of accuracy, specificity, sensitivity, precision, MSE, PSNR, PPV, NPV, quantum noise, and CDA for existing and proposed methods. *X* and *Y*-axes represent the parameters used and values obtained respectively. Red, blue, green yellow, pink, and orange colour indicate median filter, classifier, GSS filter, Kaun filter, 2D Euclidean operator, 3D convolution operator.

Figure 11 Comparison for image 4 with existing and proposed methods (see online version for colours)

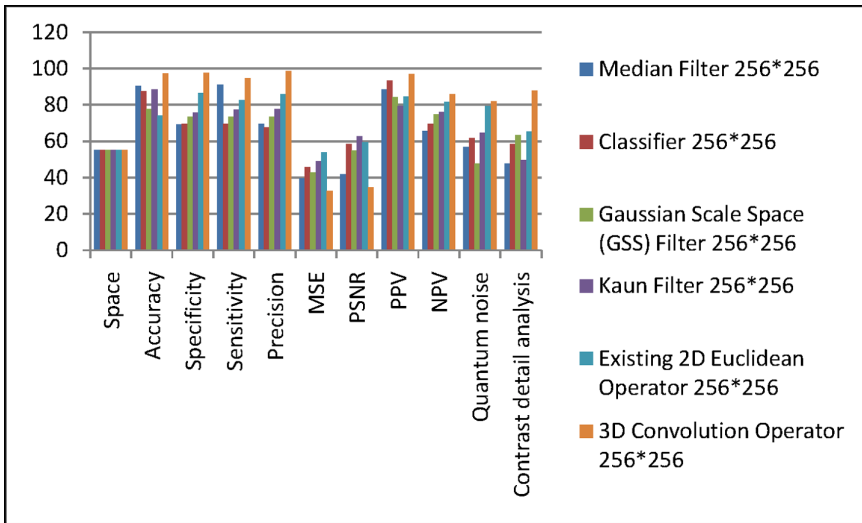


Table 5 presents the performance of existing and proposed models for various parameters with image 5 whose pixel count is 256×256 .

Table 5 Comparative performance analysis for image 5

Parameters used	Median filter	Classifier	Gaussian scale-space (GSS) filter	Kaun filter	Existing 2D Euclidean operator	3D convolution operator
Pixel Count	256*256	256*256	256*256	256*256	256*256	256*256
Space	54.8	54.8	54.8	54.8	54.8	54.8
Accuracy	86.2	90.5	72.6	83.5	86.4	98.5
Specificity	75.2	77.6	79.4	86.2	87.4	98.6
Sensitivity	68.5	71.6	75.9	79.4	82.5	96
Precision	68.6	71.5	84.3	78.6	82.6	97
MSR	53.9	62.8	56.9	60.8	58.7	39.7
PSNR	34.9	44.7	47.9	53.7	51.3	29.4
PPV	84.6	91.7	73.9	68.5	87.4	96
NPV	69.4	73.5	73.5	63.4	72.9	79
Quantum noise	63.1	58.4	72.4	68.5	73.4	79
Contrast detail analysis	78.5	84.6	81.4	67.4	73.4	92

Figure 12 shows a comparison of accuracy, specificity, sensitivity, precision, MSE, PSNR, PPV, NPV, quantum noise, and CDA for existing and proposed methods. X and Y-axis represent the parameters used and values obtained respectively. Red, blue, green yellow, pink, and orange colour indicate median filter, classifier, GSS filter, Kaun filter, 2D Euclidean operator, 3D convolution operator.

Figure 12 Comparison for image 6 with existing and proposed methods (see online version for colours)

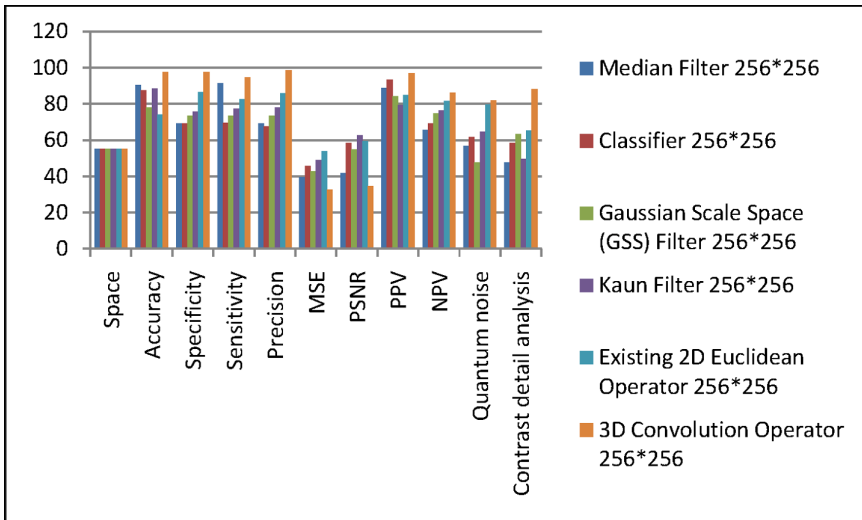


Table 6 presents the performance of existing and proposed models for various parameters with image 6 whose pixel count is 256×256 .

Table 6 Comparative performance analysis for image 6

<i>Parameters used</i>	<i>Median filter</i>	<i>Classifier</i>	<i>Gaussian scale-space (GSS) filter</i>	<i>Kaun filter</i>	<i>Existing 2D Euclidean operator</i>	<i>3D convolution operator</i>
Pixel count	256*256	256*256	256*256	256*256	256*256	256*256
Space	55.2	55.2	55.2	55.2	55.2	55.2
Accuracy	90.5	87.5	77.8	88.4	74.2	97.4
Specificity	69.3	69.4	73.6	75.8	86.4	97.6
Sensitivity	91.2	69.6	73.6	77.4	82.6	94.6
Precision	69.4	67.5	73.6	77.8	85.9	98.6
MSE	39.4	45.8	42.7	48.9	53.7	32.7
PSNR	41.9	58.4	54.7	62.7	59.4	34.6
PPV	88.6	93.4	84.3	79.2	84.7	97
NPV	65.6	69.4	74.8	76.2	81.6	86
Quantum noise	56.8	61.7	47.5	64.8	79.5	82
Contrast detail analysis	47.6	58.4	63.4	49.7	65.4	88

Figure 13 shows a comparison of accuracy, specificity, sensitivity, precision, MSE, PSNR, PPV, NPV, quantum noise, and CDA for existing and proposed methods. *X* and *Y*-axes represent the parameters used and values obtained respectively. Red, blue, green yellow, pink, and orange colour indicate median filter, classifier, GSS filter, Kaun filter, 2D Euclidean operator, 3D convolution operator. The performance of existing and proposed models for various parameters with image 4 whose pixel count is 256×256 shown in Figure 14.

Figure 13 Comparison for image 6 with existing and proposed methods (see online version for colours)

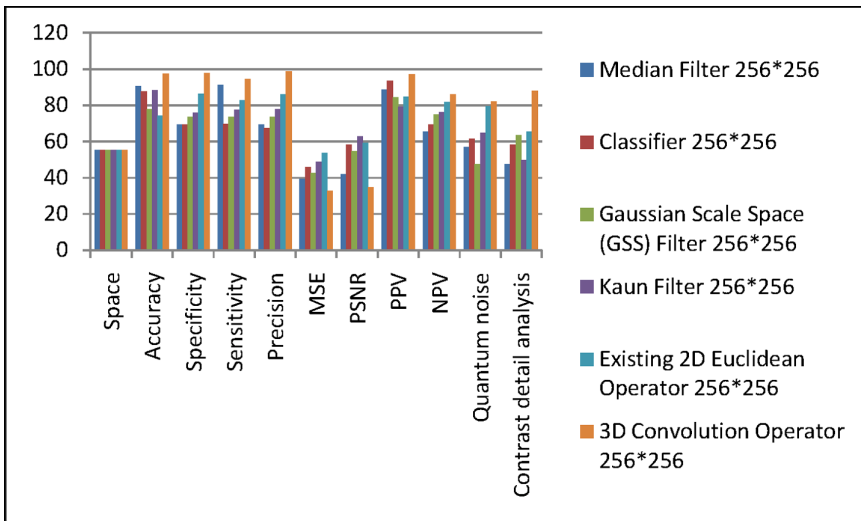
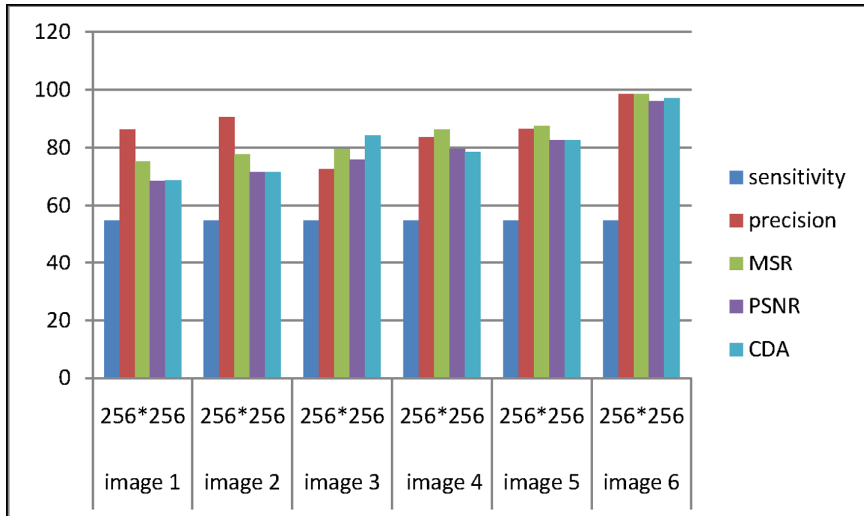


Figure 14 Overall comparison of proposed 3D convolution operator for PET smoothing (see online version for colours)

5 Conclusion

This paper describes a method for the differentiation of tumour cells from the normal cells by applying F-18 (fluorine- 18) PET (positron emission tomography) and can be smoothed using Gaussian 3D convolution operator which shows the differentiation tumour cells. The performance analysis shows images showing differentiation of tumour cells by applying F-18 PET, smoothed image using Gaussian 3D convolution operator. Comparison of accuracy graphs for Gaussian 3D convolution operator and 2D Gaussian operator, and specificity and sensitivity graphs for Gaussian 3D convolution operator shows the improved accuracy and specificity using the Gaussian 3D convolution operator.

References

- 1 Gawade, P. and Chauhan, R.P. (2016) 'Detection of lung cancer using image processing techniques', *Int. J. Adv. Technol. Eng. Explor.*, Vol. 3, No. 25, p.217.
- 2 Tiwari, A.K. (2016) 'Prediction of lung cancer using image processing techniques: a review', *An International Journal (ACIJ)*, Vol. 3, No. 1, pp.1–9.
- 3 Kaur, J., Garg, N. and Kaur, D. (2014) 'A survey of lung cancer detection techniques on CT scan images', *Int. J. Sci. Eng. Res.*, Vol. 5, No. 6.
- 4 Perumal, S. and Velmurugan, T. (2016). 'Image segmentation based survey on the lung cancer MRI images', *Int. J. Data Min. Tech. Appl.*, Vol. 5, No. 2, pp.2627–2630.
- 5 Latchoumi, T.P. and Sunitha, R. (2010) 'Multi agent systems in distributed datawarehousing', *2010 International Conference on Computer and Communication Technology (ICCCCT)*, Kerala, pp.442–447.
- 6 Naini, A.S., Patel, R.V. and Samani, A. (2010) 'CT-enhanced ultrasound image of a totally deflated lung for image-guided minimally invasive tumor ablative procedures', *IEEE Trans. Biomed. Eng.*, Vol. 57, No. 10, pp.2627–2630.

- 7 Latchoumi, T.P., Ezhilarasi, T.P. and Balamurugan, K. (2019) 'Bio-inspired weighed quantum particle swarm optimization and smooth support vector machine ensembles for identification of abnormalities in medical data', *SN Appl. Sci.*, Vol. 1, No. 10, p.1137.
- 8 Ju, W., Xiang, D., Zhang, B., Wang, L., Kopriva, I. and Chen, X. (2015) 'Random walk and graph cut for co-segmentation of lung tumor on PET-CT images', *IEEE Trans. Image Process.*, Vol. 24, No. 12, pp.5854–5867.
- 9 Latchoumi, T.P. and Parthiban, L. (2017) 'Abnormality detection using weighed particle swarm optimization and smooth support vector machine', *Biomedical Research*, Vol. 12, No. 3, pp.1–2.
- 10 Ballangan, C., Wang, X., Fulham, M., Eberl, S., Yin, Y. and Feng, D. (2011) 'Automated delineation of lung tumors in PET images based on monotonicity and a tumor-customized criterion', *IEEE Trans. Inf Technol Biomed.*, Vol. 15, No. 5, pp.691–702.
- 11 Song, Q., Bai, J., Han, D., Bhatia, S., Sun, W., Rockey, W. and Wu, X. (2013) 'Optimal co-segmentation of tumor in PET-CT images with context information', *IEEE Trans. Med. Imaging*, Vol. 32, No. 9, pp.1685–1697.
- 12 Kopriva, I., Ju, W., Zhang, B., Shi, F., Xiang, D., Yu, K., Wang, X., Bagci, U. and Chen, X. (2016) 'Single-channel sparse non-negative blind source separation method for automatic 3-D delineation of lung tumor in PET images', *IEEE J. Biomed. Health Inform.*, Vol. 21, No. 6, pp.1656–1666.
- 13 Jia, R., Eberl, S., Wen, L., Bai, J. and Feng, D.D. (2007) 'Optimal dual time point for FDG-PET in the differentiation of benign from malignant lung lesions: A simulation study', *2007 29th Annual International Conference of the IEEE Engineering in Medicine and Biology Society*, August, IEEE, Dubai, pp.4169–4172.
- 14 Zhang, H., Han, H., Liang, Z., Hu, Y., Liu, Y., Moore, W., Ma, J. and Lu, H. (2015) 'Extracting information from previous full-dose CT scan for knowledge-based Bayesian reconstruction of current low-dose CT images', *IEEE Trans. Med. Imaging*, Vol. 35, No. 3, pp.860–870.